School of Natural Sciences and Mathematics

Odd-Integer Quantum Hall States and Giant Spin Susceptibility in P -Type Few-Layer WSe_2

UT Dallas Author(s):

Zhi-qiang Bao
Cheng-Cheng Liu
Fan Zhang

Citation:

Xu, S., J. Shen, G. Long, Z. Wu, et al. 2017. "Odd-integer quantum hall states and giant spin susceptibility in p -type few-layer WSe_2." Physical Review Letters 118(6), doi:10.1103/PhysRevLett.118.067702

Odd-Integer Quantum Hall States and Giant Spin Susceptibility in p-Type Few-Layer WSe_2

Shuigang Xu,[1] Junying Shen,[1] Gen Long,[1] Zefei Wu,[1] Zhi-qiang Bao,[2] Cheng-Cheng Liu,[2] Xiao Xiao,[1] Tianyi Han,[1] Jiangxiazi Lin,[1] Yingying Wu,[1] Huanhuan Lu,[1] Jianqiang Hou,[1] Liheng An,[1] Yuanwei Wang,[1] Yuan Cai,[1] K. M. Ho,[1] Yuheng He,[1] Rolf Lortz,[1] Fan Zhang,[2,†] and Ning Wang[1,*]

[1]*Department of Physics and Center for Quantum Materials, the Hong Kong University of Science and Technology, Clear Water Bay, Hong Kong, China*

[2]*Department of Physics, University of Texas at Dallas, Richardson, Texas 75080, USA*

(Received 3 November 2016; published 10 February 2017)

We fabricate high-mobility p-type few-layer WSe_2 field-effect transistors and surprisingly observe a series of quantum Hall (QH) states following an unconventional sequence predominated by odd-integer states under a moderate strength magnetic field. By tilting the magnetic field, we discover Landau level crossing effects at ultralow coincident angles, revealing that the Zeeman energy is about 3 times as large as the cyclotron energy near the valence band top at the Γ valley. This result implies the significant roles played by the exchange interactions in p-type few-layer WSe_2, in which itinerant or QH ferromagnetism likely occurs. Evidently, the Γ valley of few-layer WSe_2 offers a unique platform with unusually heavy hole carriers and a substantially enhanced g factor for exploring strongly correlated phenomena.

DOI: 10.1103/PhysRevLett.118.067702

Subjected to a sufficiently high magnetic field B, the Hall resistance of a two-dimensional electron gas (2DEG) undergoes quantum Hall (QH) transitions to take on the quantized values $h/\nu e^2$, where h is the Planck constant, e is the elementary charge, and ν is the Landau level (LL) filling factor (FF). The effective Landé g factor g^* and the effective mass of carriers m^* are two fundamental parameters that characterize the energy gaps of LLs. In the single-particle picture, the cyclotron energy $E_c = \hbar\omega_c = \hbar eB/m^*$, reflecting the quantization of an electron's orbital motion. The Zeeman energy $E_z = g^*\mu_B B$, where μ_B is the Bohr magneton, causes the spin splitting of the LLs. In GaAs-based quantum wells, E_c is much larger than E_z, and QH effects occur only at even-integer FFs in a low-field regime. At high fields, the electron-electron interactions [1–3] can substantially lift the spin degeneracy and give rise to odd-integer FFs. In 2DEGs with comparable E_c and E_z, exotic QH states may appear. For instance, a series of even-denominator fractional QH states has been observed at a MgZnO/ZnO heterointerface [4,5] where $E_z/E_c = 0.95$. Here we report the surprising discovery of $E_z/E_c = 2.83$, the largest among all accessible 2DEGs to date, in p-type few-layer WSe_2. This feature presents a remarkable 2DEG platform with strongly correlated phenomena.

The emergence of atomically thin crystals, such as graphene [6,7], black phosphorus [8,9], and transition metal dichalcogenides (TMDCs) [10,11], has greatly enriched the prospective platforms of 2DEGs. Among these materials, TMDCs, with strong spin-orbit coupling (SOC), large band gaps, and rich valley degrees [12], exhibit several extraordinary phenomena, such as circular dichroism [13–15], the valley Zeeman effect [16–19], and the optovalley Hall effect [20]. However, because of contact problems and low carrier mobility, the investigation on TMDC QH transport has been limited until recently. In parallel with several significant efforts [10,11,21,22], two experiments observed the onset of integer QH states in TMDC devices: one for the *Q-valley electrons* [10] and the other for the *K-valley holes* [11]. In both cases, the transport features were predominated by *even-integer* QH states.

The band structures of TMDCs are thickness dependent. For WSe_2, according to the first-principles calculations [23] and angle-resolved photoemission spectroscopy (APRES) experiments [24], the valence band maxima change from the K/K' points in monolayers or bilayers to the Γ point in thicker layers. Here, we report the surprising observation of an anomalous magnetotransport of Γ-*valley holes*, predominated by *odd-integer* QH states, in high-mobility p-type few-layer WSe_2. By means of tilt-field and temperature-dependent measurements, we further evidence a LL crossing at ultralow coincident angles and discover giant spin susceptibility $\chi^* = g^*m^*\mu_B/2\pi\hbar^2 \propto g^*m^* = 5.65m_0$, where m_0 is the electron mass. This remarkable characteristic is responsible for the observed unconventional FF sequence and amounts to an enormous ratio of Zeeman-to-cyclotron energies $E_z/E_c = g^*m^*/2m_0 = 2.83$. The heavy hole carriers and the giant spin susceptibility suggest that p-type few-layer WSe_2 is a fertile ground for exploring 2D strongly correlated phenomena.

To fabricate high-mobility p-type WSe_2 devices, as illustrated in Figs. 1(a) and 1(b), we employ h-BN encapsulated structures and a dry transfer technique [22,25]. To access the Γ valley (p-type) of WSe_2, we deposit a contact metal Pd through the selective etching technique [22,26].

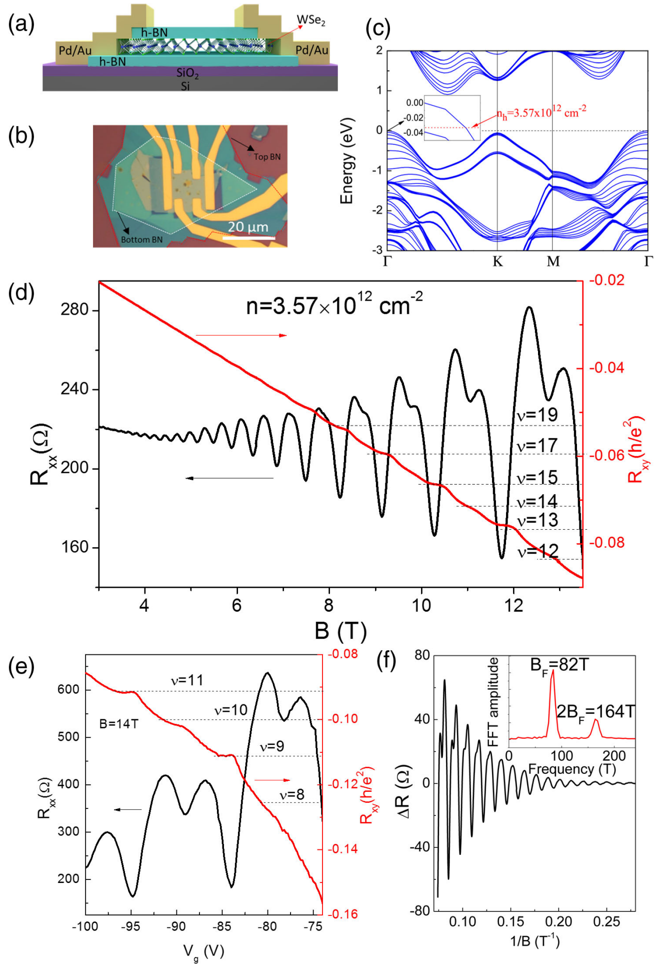

FIG. 1. (a) Schematic of h-BN encapsulated WSe_2 structures. (b) Optical image of a Hall device in our measurement. (c) Calculated band structure of eight-layer WSe_2 . (d) R_{xy} and corresponding R_{xx} as functions of B measured at 1.7 K for a hole density of 3.57×10^{12} cm^{-2}. The Fermi level for (d) crosses only the highest spin-degenerate sub-band at the Γ valley in (c). (e) R_{xy} and R_{xx} as functions of V_g at 14 T. The dashed lines mark the values of the quantized Hall plateaus ($h/\nu e^2$). (f) Background subtracted magnetoresistance as a function of $1/B$ at $n = 3.57 \times 10^{12}$ cm^{-2}. The inset is the corresponding FFT.

The reason is that the work function of Pd (~5.6 eV) [27] matches the valence band edge of WSe_2 (~5.2 eV) [28] and forms a low barrier with p-type WSe_2, which is confirmed by the I_{ds}-V_{ds} curves (Fig. S1 [29]). The typical field-effect mobility μ_F achieved in our samples is about 220 $\mathrm{cm}^2/\mathrm{V\,s}$ at room temperature and 12 000 $\mathrm{cm}^2/\mathrm{V\,s}$ at 2 K. The Hall mobility μ_H ($\mu_H = \sigma/ne$ with σ the sheet conductance and n the carrier density determined by Hall measurements) is about 4800 $\mathrm{cm}^2/\mathrm{V\,s}$ ($n = 4.1 \times 10^{12}$ cm^{-2}) at 2 K. Similar to other 2D semiconductors [30], the measured μ_H is lower than μ_F, originating from the carrier density dependence of μ_H.

Examples of longitudinal resistance (R_{xx}) and Hall resistance (R_{xy}) measured as functions of the magnetic field (B) at fixed carrier densities are shown in Fig. 1(d). At low B, pronounced Shubnikov–de Haas (SdH) oscillations are clearly visible. From the onset of SdH oscillations (3.5 T), we can estimate the quantum mobility $\mu_q \approx 1/B_q = 2800$ $\mathrm{cm}^2/\mathrm{V\,s}$ [31], further confirming the high quality of our sample. We can also extract the hole density participating in the oscillations using $n = g_s g_v e B_F/h$, where g_s and g_v are the spin and valley degeneracies, respectively, and B_F is the oscillation frequency. B_F can be extracted from the fast Fourier transform (FFT) in Fig. 1(f). The carrier densities of our samples are rather low, and the Fermi energies are located near the valence band maxima, i.e., the Brillouin zone center (Γ point) with $g_s = 2$ and $g_v = 1$, as shown in Fig. 1(c). The hole densities obtained from the oscillations are found to be consistent with those obtained from Hall measurements (Fig. S3 [29]).

Similar to the characteristics of QH effects observed in other 2DEGs, as shown in Fig. 1(d), the appearance of quantized R_{xy} plateaus is accompanied by the exhibition of local R_{xx} minima with $R_{xx} \ll R_{xy}$ [32]. Counterintuitively, the QH states with odd-integer FFs, such as $\nu = 19$, 17, 15, and 13, already appear sequentially at low B, whereas the states with even-integer FFs, such as $\nu = 14$, 12, and 10, appear only at high B. A similar phenomenon was reported for the QH states in a polar oxide heterostructure [4,32]. The sequence of the observed FFs usually reflects E_z/E_c. As $E_z/E_c = m^* g^*/2m_0$, it provides a measure of the spin susceptibility $\chi^* \propto g^* m^*$. In GaAs or graphene 2DEGs [33,34], E_z/E_c is normally on the order of 10^{-2} because of the small m^* and g factor. Accordingly, the LLs with the same orbital index but opposite spins are nearly degenerate at low B and become split only at sufficiently high B, when the Zeeman effect is enhanced by electron-electron interactions [1–3]. Therefore, in these conventional systems, the even-integer QH states appear first, followed by odd-integer states, as the B increases.

In light of the above analysis, the unconventional sequence of QH states in few-layer WSe_2 is strongly suggestive of χ^* being rather large. A simple analysis reveals that the odd-integer QH states predominate under low fields when $2j + 0.5 < E_z/E_c < 2j + 1.5$, with j being a non-negative integer. Hence, we tilt B to study the LL crossing, which has been a standard method to determine E_z/E_c [2].

Under a tilted B, E_c scales with the perpendicular field $B_\perp$, whereas E_z scales with the total field B_{tot}. Therefore, tuning the tilt angle θ can increase the ratio E_z/E_c and produce the crossing of LLs. As illustrated in Fig. 2(e), the evolution of the LL crossing is characterized by $i = E_z/E_c = g^* \mu_B B_{\mathrm{tot}}/(\hbar e B_\perp/m^*)$. As $B_\perp = B_{\mathrm{tot}} \cos\theta$ and $\mu_B = \hbar e/(2m_0)$,

$$i \cos\theta = g^* m^*/2m_0. \tag{1}$$

As θ increases, two LLs with opposite spins and orbital indices differing by i cross each other at the so-called coincidence angles, where i takes integer values.

Figure 2(a) displays the experimental data of the SdH oscillations at different tilt angles. For a fixed θ, R_{xx} and R_{xy} are recorded as functions of B_{tot}. The value of θ is calibrated by the simultaneous R_{xy} measurements in the nonquantized regime, as the total carrier density does not change upon θ. At $\theta = 0°$, the QH states with odd- and even-integer FFs are both observed at high B. As θ increases, the even-integer QH states at $\nu = 16$, 18, and 20 at high B become weaker and weaker and eventually vanish at the coincidence angle of 23.6°. Conversely, the odd-integer QH states change little. In other words, pronounced SdH minima (maxima) for the odd- (even-) integer states are observed at $\theta = 23.6°$. When θ is tilted beyond 23.6°, the even-integer QH states gradually appear again at $\nu = 26$, 28, and 30, whereas the odd-integer QH states at $\nu = 25$, 27, and 29 gradually disappear. At the second coincidence angle of 45.9°, pronounced SdH minima (maxima) for the even- (odd-) integer states are clearly observed, opposite to the case for $\theta = 23.6°$. Likewise, the next-order phase reversal [35] in the SdH oscillations is observed at the coincidence angle of 54.8°.

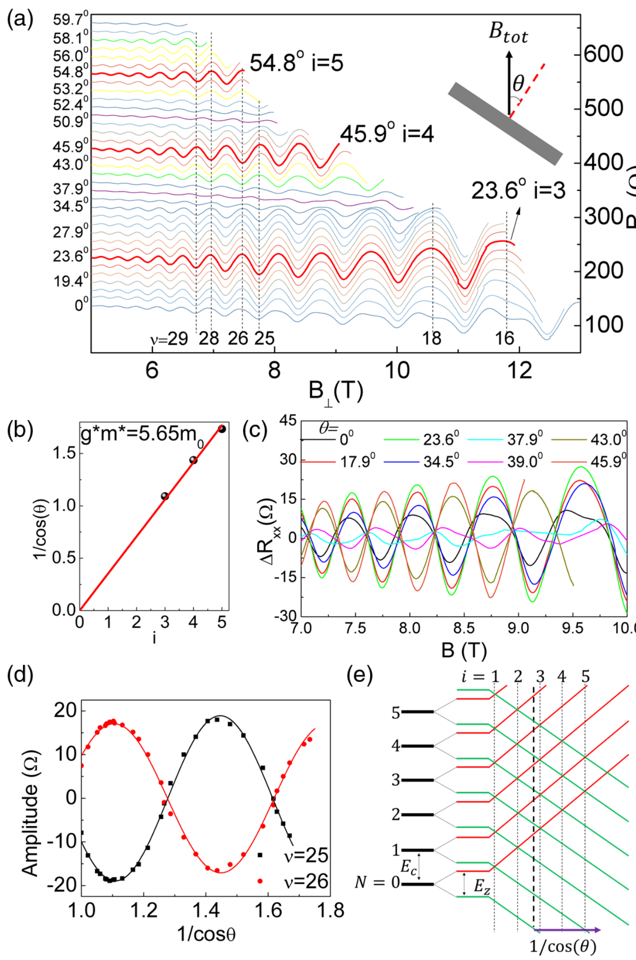

FIG. 2. (a) R_{xx} as a function of $B_\perp$ at various tilted angles at 1.7 K. The inset shows the illustration of the angles. Data were recorded at a fixed V_g and shifted vertically for clarity. Coincidences at $i = 3$, 4, 5 are emphasized as bold lines. (b) $1/\cos\theta$ of the identified coincidence angles as a function of i. (c) Comparison of SdH amplitudes at various tilted angles from the first ($i = 3$) to the second ($i = 4$) coincident angle. Smooth backgrounds were subtracted for each line. (d) Evolution of SdH oscillation amplitudes as a function of $1/\cos\theta$ at FFs of $\nu = 25$ and 26. The solid curves are the fitted cosine functions in Eq. (2). (e) Schematic of spin-split LLs as a function of the tilted angle for a constant $B_\perp$. The black dashed line marks the location of $\theta = 0°$.

We employ Eq. (1) to fit the three identified coincidence angles with respect to three adjacent integers in Fig. 2(b). Surprisingly, the coincidence angles for $\theta = 23.6°$, 45.9°, and 54.8° correspond to $i = 3$, 4, and 5, respectively. For GaAs, graphene, ZnO, and black phosphorus [4,8,36], the fitted i values all start from 1. Here, if we assign the coincidence angle $\theta = 23.6°$ to $i = 1$ (or $i = 2$), the next-order coincidence angle will be $\theta = 62.7°$ (or $\theta = 52.3°$), which largely deviates from our observation $\theta = 45.9°$ in Fig. 2(a). Therefore, the fitting appears to be unique in light of Eq. (1). Markedly, with the identified θ and i values, Eq. (1) yields $g^*m^* = 5.65m_0$, which is larger than those of the aforementioned 2DEGs. This result implies giant spin susceptibility in the p-type few-layer WSe_2.

Alternatively, we can also extract the value of g^*m^* by analyzing the dependence of the SdH oscillation amplitudes on the tilt angles, as shown in Fig. 2(c). The amplitude of SdH oscillations can be described by the Lifshitz-Kosevich formula [30]:

$$\Delta R_{xx} = A_0 R_T R_D R_S \cos\left(2\pi \frac{B_F}{B_\perp} - \pi + \varphi\right)$$
$$\text{with } R_S = \cos\left(\frac{\pi}{2}\frac{g^* m^*}{m_0}\frac{B_{\mathrm{tot}}}{B_\perp}\right), \tag{2}$$

where A_0 is a constant, R_T is the temperature factor, R_D is the Dingle factor, and R_S is the spin damping factor of Zeeman splitting. The Berry phase φ is found to be zero (Fig. S4 [29]), which is consistent with the single-band picture revealed by our first-principles calculations. At fixed temperature and $B_\perp$, the B_{tot} dependence of the SdH amplitude is determined [37] by R_S. As shown in Fig. 2(d), the observed SdH amplitudes as functions of $1/\cos\theta = B_{\mathrm{tot}}/B_\perp$ at $\nu = 25$ and 26 are well reproduced by Eq. (2) with $g^*m^* = 5.93m_0$ for $\nu = 25$ and $g^*m^* = 5.84m_0$ for $\nu = 26$.

The effective hole mass m^* can be determined by the temperature dependence of SdH oscillations. The temperature-induced damping in Eq. (2) is [26,30] $R_T = \xi/\sinh(\xi)$, where $\xi = 2\pi^2 k_B T/\hbar\omega_c$ and k_B is the Boltzmann constant. The SdH oscillations at different temperatures, for a fixed carrier concentration and $B < 9$ T, are shown in Fig. 3(a). The corresponding FFT confirms the single SdH oscillation frequency. By fitting ΔR_{xx} as a function of T using R_T, we obtain the hole cyclotron mass $m^* = 0.89m_0$, indicating $g^* = 6.35$.

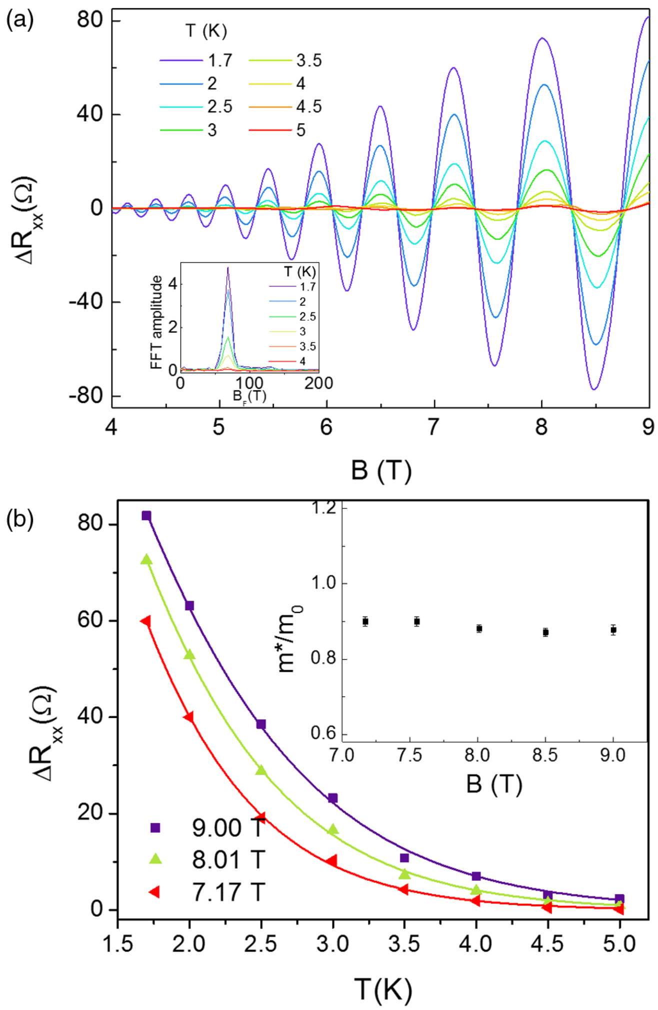

FIG. 3. (a) ΔR_{xx} as a function of B measured at various temperatures with fixed V_g. The inset is the FFT corresponding to ΔR_{xx} vs $1/B$ data. The single SdH oscillation frequency confirms no observed Zeeman splitting at low B. (b) SdH oscillation amplitudes as functions of the temperature at different B. The solid lines are the fitted curves of R_T. The inset shows the fitted hole effective masses at various B.

The band structures of few-layer WSe_2 are thickness dependent. Different from those at K valleys, the m^* at Γ valleys of WSe_2 has been confirmed to vary from $0.5m_0$ in 3D bulk to $2.8m_0$ in monolayers and affected by interlayer interactions [24,38–40]. Since our samples are about eight layers thick, we perform first-principles calculations to examine the band structure of eight-layer WSe_2, as shown in Fig. 1(c). Our calculated m^* is isotropic and $\sim 0.76m_0$, which is consistent with our measurement. As the relevant subband mainly arises from the delocalized out-of-plane $5d_z^2$ orbitals of W atoms, the SOC is negligibly weak, thus implying $g^* = 2$ according to Roth's formula [41]. Apparently, this band structure result is smaller than the experimental value of g^*. The discrepancy is likely due to the exchange interactions of holes, as will be elaborated below.

Having established that at a zero tilt angle $E_z/E_c = g^* m^*/2m_0 = 2.83$, we conclude that, surprisingly, the LL crossing among those with different orbital indices already exists when $\theta = 0°$. Specifically, as $2.5 < E_z/E_c < 3.5$, the integer QH plateaus should follow the sequence of $\nu = 1, 2, 3, 5, 7, 9, 11, \ldots, (2M+1), \ldots$ at small fields, in which the Nth LL with a downward spin and the $(N+3)$th LL with an upward spin are nearly degenerate [Fig. 4(a)]. The gap between the two nearly degenerate LLs scales linearly with B and becomes sufficiently large at high fields, in which the even-integer QH states with large orbital indices can be fully resolved. The QH plateaus exhibited in Fig. 1 are consistent with such a physical picture.

According to the LL structure in Fig. 4(a), the energy gaps at odd ($\nu = 3, 5, 7, \ldots$) and even ($\nu = 4, 6, 8, \ldots$) FFs can be, respectively, expressed by

$$\Delta_1 = E_z - 2E_c - \Gamma \quad \text{and} \quad \Delta_2 = 3E_c - E_z - \Gamma, \tag{3}$$

where Γ is the LL broadening caused by disorder. To determine the energy gaps, we measure the temperature dependence of R_{xx} as a function of V_g at a fixed B. Figure 4(b) displays the typical results for the $\nu = 11$ and 12 states at $B = 13$ T. Figures 4(c) and 4(d) further plot the $1/T$ dependence of R_{xx} minima at various B. As the energy gaps Δ_1 and Δ_2 can be approximated to the corresponding activation gaps, we deduce them by considering $R_{xx} \propto \exp(-\Delta/2k_BT)$, where the activation gap Δ can be extracted from the Arrhenius plots in Figs. 4(c) and 4(d). As clearly shown in Fig. 4(e), the measured activation gaps at $\nu = 11$ and 12 both scale linearly with the B. By relating the two fitted lines in Fig. 4(e) to Eq. (3), we obtain $E_c = 1.69B$ K and $E_z = 4.38B$ K, which lead to an effective mass $m^* = 0.80m_0$ and a g factor $g^* = 6.52$. These results are consistent with those obtained from the coincident technique and Dingle plot.

The previously reported TMDC QH states in n-type few layers and p-type mono- and bilayers are in sharp contrast to the ones studied here in p-type few layers. In the former case, the QH transport emerges from the six Q valleys [10,22], where strong SOC and inversion symmetry (asymmetry) lead to $g_s = 2$ (1) for even (odd) layers. In the latter case, the QH transport was attributed to the two K valleys [11,42]. In the present case, however, the single Γ valley with $g_s = 2$ and negligible SOC is the one that governs the QH transport. The observed QH states were predominantly at even-integer FFs in the previous two, whereas the odd-integer QH states dominate in the present study. This unexpected observation uncovers the giant spin susceptibility $\chi^* \propto g^* m^* = 5.65m_0$ in p-type few-layer WSe_2.

Given the weak interlayer couplings in WSe_2, one may wonder whether or not only the top-layer carriers participate in the quantum transport in our devices. The odd-integer QH states are predicted to predominantly occur in p-type monolayers [42], in which the mirror symmetry and

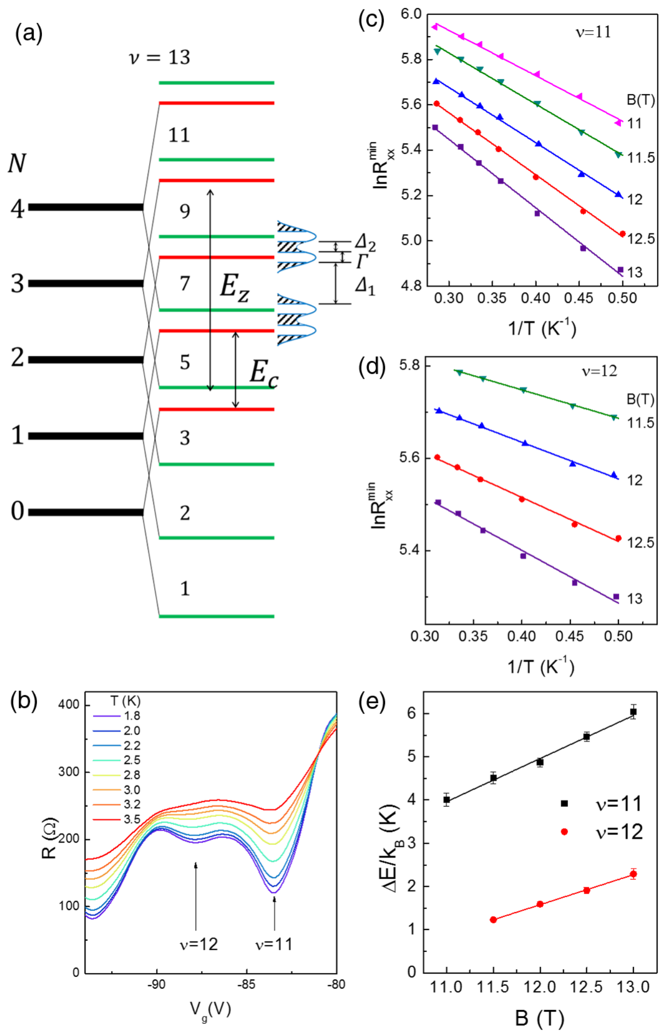

FIG. 4. (a) Schematic of LLs at the zero tilt angle. The activation gaps at the odd and even FFs (Δ_1 and Δ_2, respectively) with the LL broadening Γ are marked. (b) R_{xx} as a function of the V_g at $B = 13$ T at different temperatures. The arrows mark the $\nu = 11$ and 12 minima. (c),(d) Arrhenius plots of R_{xx} for the gaps at $\nu = 11$ and 12 at different B. Linear fits of the data yield the corresponding gaps Δ_1 and Δ_2. (e) Energy gaps as functions of B at $\nu = 11$ and 12 deduced from the Arrhenius plots. The linear fits yield the effective mass and g factor.

the strong SOC dictate a large out-of-plane spin splitting. However, this explanation can be excluded, as the SdH oscillations in Fig. 2(a) are highly sensitive to B_{tot} at fixed $B_\perp$. This analysis leaves the electron-electron interactions as the seemingly only possible explanation for the enhanced g factor. For long-range interactions, the exchange energy decreases rapidly with increasing LL orbital index and scales with $B_\perp^{1/2}$, different with the orbital independence and the linear scaling in Fig. 2(b). The $5d$ orbital relevant for Γ-valley holes is, in fact, more localized than with the p orbitals in GaAs or graphene. It is thus reasonable to speculate on the short-range interactions, the exchange energy of which scales with $B_\perp$ for each occupied LL. Nevertheless, the observed odd-integer states are all QH ferromagnets with uneven populations of spin-up and -down LLs.

Two implications follow from the determined large effective mass m^* for Γ-valley holes of WSe_2. First, the cyclotron energy is reduced by a factor of approximately 10, compared with the typical value in GaAs-based 2DEGs. This implication explains why higher mobilities are required to observe the onset of QH effects in TMDC 2DEGs. Second, the density of states, which is linearly proportional to m^*, and the interactions of $5d$ holes are both substantial. Following the Stoner criterion, itinerant ferromagnetism may exist in p-type few-layer WSe_2, thus suggesting an already established Zeeman splitting at $B = 0$. This possibility is indeed consistent with our observed coincidence angles, and yields the same value of $g^* m^*$, if the integer i's in Eq. (1) are fitted to 1, 2, and 3 or 2, 3, and 4, instead of 3, 4, and 5 (Fig. S7 [29]).

In summary, we observed an unconventional sequence of Γ-valley QH states in high-mobility WSe_2, predominantly at odd-integer FFs. The observed Hall plateaus, LL crossing, SdH amplitudes, and activation gaps are in good harmony with each other, discovering the giant spin susceptibility $\chi^* \propto g^* m^* = 5.65 m_0$. This feature implies the significant roles played by the electron-electron exchange interactions in p-type few-layer WSe_2, in which itinerant ferromagnetism or QH ferromagnetism likely occurs. Remarkably, the Γ valley of few-layer WSe_2 offers an unprecedented 2DEG platform with unusually heavy hole carriers and a large g factor for exploring strongly correlated phenomena.

We acknowledge the financial support from the Research Grants Council of Hong Kong (Projects No. 16302215, No. HKU9/CRF/13G, No. 604112, and No. N_HKUST613/12) and the UT-Dallas Research Enhancement Funds. We are grateful for the technical support of the Raith-HKUST Nanotechnology Laboratory for the electron-beam lithography facility at MCPF. F. Z. is grateful to Xiaoyan Shi for the valuable suggestions on the tilt field measurement and to Kavli Institute for Theoretical Physics for hospitality during the finalization of this work, which was supported in part by NSF Grant No. PHY11-25915.

S. X. and J. S. contributed equally to this work.

*Corresponding author.
phwang@ust.hk
†Corresponding author.
zhang@utdallas.edu

[1] S. M. Girvin, Phys. Today **53**, No. 6, 39 (2000).
[2] R. J. Nicholas, R. J. Haug, K. v. Klitzing, and G. Weimann, Phys. Rev. B **37**, 1294 (1988).
[3] J. F. Janak, Phys. Rev. **178**, 1416 (1969).

[4] J. Falson, D. Maryenko, B. Friess, D. Zhang, Y. Kozuka, A. Tsukazaki, J. H. Smet, and M. Kawasaki, Nat. Phys. **11**, 347 (2015).
[5] C. R. Dean, Nat. Phys. **11**, 298 (2015).
[6] K. S. Novoselov, A. K. Geim, S. V. Morozov, D. Jiang, M. I. Katsnelson, I. V. Grigorieva, S. V. Dubonos, and A. A. Firsov, Nature (London) **438**, 197 (2005).
[7] Y. Zhang, Y.-W. Tan, H. L. Stormer, and P. Kim, Nature (London) **438**, 201 (2005).
[8] L. Li, F. Yang, G. J. Ye, Z. Zhang, Z. Zhu, W. Lou, X. Zhou, L. Li, K. Watanabe, T. Taniguchi, K. Chang, Y. Wang, X. H. Chen, and Y. Zhang, Nat. Nanotechnol. **11**, 593 (2016).
[9] G. Long, D. Maryenko, J. Shen, S. Xu, J. Hou, Z. Wu, W. K. Wong, T. Han, J. Lin, Y. Cai, R. Lortz, and N. Wang, Nano Lett. **16**, 7768 (2016).
[10] Z. Wu, S. Xu, H. Lu, A. Khamoshi, G.-B. Liu, T. Han, Y. Wu, J. Lin, G. Long, Y. He, Y. Cai, Y. Yao, F. Zhang, and N. Wang, Nat. Commun. **7**, 12955 (2016).
[11] B. Fallahazad, H. C. P. Movva, K. Kim, S. Larentis, T. Taniguchi, K. Watanabe, S. K. Banerjee, and E. Tutuc, Phys. Rev. Lett. **116**, 086601 (2016).
[12] X. Xu, W. Yao, D. Xiao, and T. F. Heinz, Nat. Phys. **10**, 343 (2014).
[13] H. Zeng, J. Dai, W. Yao, D. Xiao, and X. Cui, Nat. Nanotechnol. **7**, 490 (2012).
[14] K. F. Mak, K. He, J. Shan, and T. F. Heinz, Nat. Nanotechnol. **7**, 494 (2012).
[15] T. Cao, G. Wang, W. Han, H. Ye, C. Zhu, J. Shi, Q. Niu, P. Tan, E. Wang, B. Liu, and J. Feng, Nat. Commun. **3**, 887 (2012).
[16] A. Srivastava, M. Sidler, A. V. Allain, D. S. Lembke, A. Kis, and A. Imamoglu, Nat. Phys. **11**, 141 (2015).
[17] Y. Li, J. Ludwig, T. Low, A. Chernikov, X. Cui, G. Arefe, Y. D. Kim, A. M. van der Zande, A. Rigosi, H. M. Hill, S. H. Kim, J. Hone, Z. Li, D. Smirnov, and T. F. Heinz, Phys. Rev. Lett. **113**, 266804 (2014).
[18] G. Aivazian, Z. Gong, A. M. Jones, R.-L. Chu, J. Yan, D. G. Mandrus, C. Zhang, D. Cobden, W. Yao, and X. Xu, Nat. Phys. **11**, 148 (2015).
[19] D. MacNeill, C. Heikes, K. F. Mak, Z. Anderson, A. Kormányos, V. Zólyomi, J. Park, and D. C. Ralph, Phys. Rev. Lett. **114**, 037401 (2015).
[20] K. F. Mak, K. L. McGill, J. Park, and P. L. McEuen, Science **344**, 1489 (2014).
[21] X. Cui, G.-H. Lee, Y. D. Kim, G. Arefe, P. Y. Huang, C.-H. Lee, D. A. Chenet, X. Zhang, L. Wang, F. Ye, F. Pizzocchero, B. S. Jessen, K. Watanabe, T. Taniguchi, D. A. Muller, T. Low, P. Kim, and J. Hone, Nat. Nanotechnol. **10**, 534 (2015).
[22] S. Xu, Z. Wu, H. Lu, Y. Han, G. Long, X. Chen, T. Han, W. Ye, Y. Wu, J. Lin, J. Shen, Y. Cai, Y. He, F. Zhang, R. Lortz, C. Cheng, and N. Wang, 2D Mater. **3**, 021007 (2016).
[23] H. Zeng, G.-B. Liu, J. Dai, Y. Yan, B. Zhu, R. He, L. Xie, S. Xu, X. Chen, W. Yao, and X. Cui, Sci. Rep. **3**, 1608 (2013).
[24] N. R. Wilson, P. V. Nguyen, K. L. Seyler, P. Rivera, A. J. Marsden, Z. P. L. Laker, G. C. Constantinescu, V. Kandyba, A. Barinov, N. D. M. Hine, X. Xu, and D. H. Cobden, arXiv:1601.05865.
[25] L. Wang, I. Meric, P. Y. Huang, Q. Gao, Y. Gao, H. Tran, T. Taniguchi, K. Watanabe, L. M. Campos, D. A. Muller, J. Guo, P. Kim, J. Hone, K. L. Shepard, and C. R. Dean, Science **342**, 614 (2013).
[26] X. Chen, Y. Wu, Z. Wu, Y. Han, S. Xu, L. Wang, W. Ye, T. Han, Y. He, Y. Cai, and N. Wang, Nat. Commun. **6**, 7315 (2015).
[27] N. E. Singh-Miller and N. Marzari, Phys. Rev. B **80**, 235407 (2009).
[28] S. McDonnell, A. Azcatl, R. Addou, C. Gong, C. Battaglia, S. Chuang, K. Cho, A. Javey, and R. M. Wallace, ACS Nano **8**, 6265 (2014).
[29] See Supplemental Material at http://link.aps.org/supplemental/10.1103/PhysRevLett.118.067702 for details on experimental methods, output characteristics, mobility and carrier density measurements, Berry phase, and LL crossing in fixed B_{tot}.
[30] L. Li, G. J. Ye, V. Tran, R. Fei, G. Chen, H. Wang, J. Wang, K. Watanabe, T. Taniguchi, L. Yang, X. H. Chen, and Y. Zhang, Nat. Nanotechnol. **10**, 608 (2015).
[31] A. S. Mayorov, D. C. Elias, I. S. Mukhin, S. V. Morozov, L. A. Ponomarenko, K. S. Novoselov, A. K. Geim, and R. V. Gorbachev, Nano Lett. **12**, 4629 (2012).
[32] A. Tsukazaki, A. Ohtomo, T. Kita, Y. Ohno, H. Ohno, and M. Kawasaki, Science **315**, 1388 (2007).
[33] D. C. Tsui and A. C. Gossard, Appl. Phys. Lett. **38**, 550 (1981).
[34] Y. Zhang, Z. Jiang, J. P. Small, M. S. Purewal, Y. W. Tan, M. Fazlollahi, J. D. Chudow, J. A. Jaszczak, H. L. Stormer, and P. Kim, Phys. Rev. Lett. **96**, 136806 (2006).
[35] F. F. Fang and P. J. Stiles, Phys. Rev. **174**, 823 (1968).
[36] A. Tsukazaki, A. Ohtomo, M. Kawasaki, S. Akasaka, H. Yuji, K. Tamura, K. Nakahara, T. Tanabe, A. Kamisawa, T. Gokmen, J. Shabani, and M. Shayegan, Phys. Rev. B **78**, 233308 (2008).
[37] E. V. Kurganova, H. J. van Elferen, A. McCollam, L. A. Ponomarenko, K. S. Novoselov, A. Veligura, B. J. van Wees, J. C. Maan, and U. Zeitler, Phys. Rev. B **84**, 121407 (2011).
[38] W. Jin, P.-C. Yeh, N. Zaki, D. Zhang, J. T. Sadowski, A. Al-Mahboob, A. M. van der Zande, D. A. Chenet, J. I. Dadap, I. P. Herman, P. Sutter, J. Hone, and R. M. Osgood, Phys. Rev. Lett. **111**, 106801 (2013).
[39] H. Yuan, Z. Liu, G. Xu, B. Zhou, S. Wu, D. Dumcenco, K. Yan, Y. Zhang, S.-K. Mo, P. Dudin, V. Kandyba, M. Yablonskikh, A. Barinov, Z. Shen, S. Zhang, Y. Huang, X. Xu, Z. Hussain, H. Y. Hwang, Y. Cui, and Y. Chen, Nano Lett. **16**, 4738 (2016).
[40] H. Peelaers and C. G. Vande Walle, Phys. Rev. B **86**, 241401 (2012).
[41] L. M. Roth, B. Lax, and S. Zwerdling, Phys. Rev. **114**, 90 (1959).
[42] X. Li, F. Zhang, and Q. Niu, Phys. Rev. Lett. **110**, 066803 (2013).